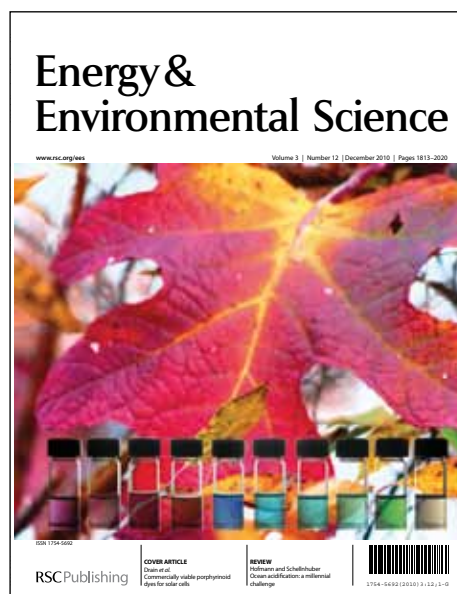


Energy & Environmental Science

Accepted Manuscript



This is an *Accepted Manuscript*, which has been through the RSC Publishing peer review process and has been accepted for publication.

Accepted Manuscripts are published online shortly after acceptance, which is prior to technical editing, formatting and proof reading. This free service from RSC Publishing allows authors to make their results available to the community, in citable form, before publication of the edited article. This *Accepted Manuscript* will be replaced by the edited and formatted *Advance Article* as soon as this is available.

To cite this manuscript please use its permanent Digital Object Identifier (DOI®), which is identical for all formats of publication.

More information about *Accepted Manuscripts* can be found in the [Information for Authors](#).

Please note that technical editing may introduce minor changes to the text and/or graphics contained in the manuscript submitted by the author(s) which may alter content, and that the standard [Terms & Conditions](#) and the [ethical guidelines](#) that apply to the journal are still applicable. In no event shall the RSC be held responsible for any errors or omissions in these *Accepted Manuscript* manuscripts or any consequences arising from the use of any information contained in them.

Cite this: DOI: 10.1039/c0xx00000x

www.rsc.org/xxxxxx

ARTICLE TYPE

Inherent Electronic Trap States in TiO₂ Nanocrystals: Effect of Saturation and Sintering

Francesca Nunzi,^{*a,b} Edoardo Mosconi,^a Lorian Storchi,^b Enrico Ronca,^{a,b} Annabella Selloni,^c Michael Grätzel^d and Filippo De Angelis^{a*}

Received (in XXX, XXX) Xth XXXXXXXXX 20XX, Accepted Xth XXXXXXXXX 20XX
DOI: 10.1039/b000000x

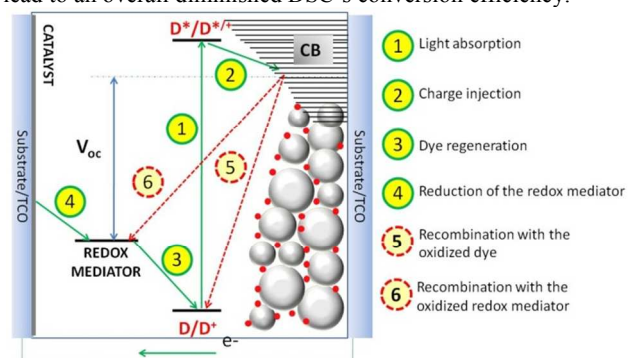
We report a quantum mechanical investigation on the nature of electronic trap states in realistic models of individual and sintered anatase TiO₂ nanocrystals (NCs) of ca. 3 nm diameter. We find unoccupied electronic states of lowest energy to be localized within the central part of the NCs, and to originate from under-coordinated surface Ti atoms lying mainly at the edges between the (100) and (101) facets. These localized states are found at about 0.3-0.4 eV below the fully delocalized conduction band states, in good agreement with both electrochemical and spectro-electrochemical results. The overall Density-Of-States (DOS) below the conduction band (CB) can be accurately fitted to an exponential distribution of states, in agreement with capacitance data. Water molecules adsorbed on the NCs surface raise the energy and reduce the number of localized states, thus modifying the DOS. As a possible origin of additional trap states, we further investigated the oriented attachment of two TiO₂ NCs at various possible interfaces. For the considered models, we found only minor differences between the DOS of two interacting NCs and those of the individual constituent NCs. Our results point at the presence of inherent trap states even in perfectly stoichiometric and crystalline TiO₂ NCs due to the unavoidable presence of under-coordinated surface Ti(IV) ions at the (100) facets.

1 Introduction

Dye-sensitized solar cells (DSCs) represent a promising approach to the direct conversion of sunlight into electrical energy at low cost and high efficiency.¹⁻⁵ DSCs are based on a dye-sensitized mesoporous oxide layer, usually composed by a network of sintered anatase TiO₂ nanoparticles (typically ~20 nm in size), interpenetrated by a liquid redox electrolyte (typically I⁻/I₃⁻ or Co(II)/Co(III)-polypyridine complexes in a volatile organic solvent), Scheme 1. Upon photoexcitation of the chemisorbed dye, electrons are injected into the oxide manifold of unoccupied states and can travel across the TiO₂ nanoparticle network until they are collected at the transparent conducting glass back contact. The oxidized dye is regenerated by the redox electrolyte. The circuit is closed by electrolyte regeneration at the counter-electrode, see processes 1-4 in Scheme 1.

Recently, DSCs efficiencies exceeding 12 % have been obtained,⁶ although still higher values are needed to effectively compete with conventional photovoltaics. A main DSCs efficiency bottleneck is the recombination of injected electrons with oxidized species in the electrolyte and with oxidized dye molecules, processes 5 and 6 in Scheme 1. Usually recombination with the oxidized dye is prevented by the fast dye regeneration rate by the reduced species, e.g. I⁻ or Co(II), in the electrolyte.³ Since electron collection at the electrode competes with recombination at the TiO₂/electrolyte interface, slow electron

transport can limit the charge-collection efficiency and eventually lead to an overall diminished DSC's conversion efficiency.^{7,8}



Scheme 1. Schematic representation of the constituent materials and energy levels of a DSC along with forward (green lines) and backward (dotted red lines) electronic processes. The energy levels roughly correspond to those of a DSC based on the N3 dye (red spots), TiO₂ nanoparticles (grey spheres) and I⁻/I₃⁻ redox mediator (not shown).

Due to the absence of a significant electric potential gradient in the semiconductor film, electron transport in mesoporous TiO₂ is believed to proceed by diffusion,⁷⁻¹⁴ usually described by an effective diffusion coefficient (D_{eff}).^{7,14-17} For nanostructured TiO₂ films commonly employed in DSCs, D_{eff} values in the range 10^{-8} - 10^{-4} cm²/s have been measured, depending on the light intensity. These values are orders of magnitude smaller than those observed for TiO₂ single crystals,^{9,10,14,18} suggesting a high

concentration of electron-trapping sites in the semiconductor film.¹⁹⁻²⁶

Intense research efforts have been devoted to characterize the electronic trap states in single crystal and colloidal TiO₂.²⁷⁻³⁰ Early studies³¹⁻³⁴ recognized the presence of various types of traps, with energy levels ranging from 0.2 to 0.9 eV below the nominal conduction band (CB) edge. Bisquert et al.^{23-25,35} classified the electronic states in TiO₂ as: *i*) conduction band states (or transport states or extended states) responsible for effective electron transport; *ii*) bulk traps, i.e. localized electronic states that trap and release electrons from and to the CB only, and *iii*) surface traps, i.e. localized electronic states that trap/release electrons from/to both the CB and acceptor species in solution. Hagfeldt and co-workers³⁶ using photoelectron spectroscopy measured a broad distribution of trap states centered ca. 1 eV below the CB edge of a nanostructured TiO₂ film. Spectroelectrochemistry measurements by Fitzmaurice and coworkers³⁷ evaluated the effect of the electrolyte solution on the flat band potentials of mesoporous nanocrystalline TiO₂ electrodes.³⁸ These studies suggested that in mesoporous TiO₂ films, the CB has a low energy tail of localized states below the energy characterizing the onset of fully delocalized conduction band states (also termed mobility edge). Kavan et al.³⁹ and many others since then⁴⁰⁻⁴⁹ proposed the existence of deep, surface trap states in the band gap, below the most significant portion of the exponential tail of the DOS. In the presence of a broad distribution of localized states, electronic transport is described within the multiple trapping model,⁵⁰⁻⁵⁷ in which transport through the extended CB states above the mobility edge is slowed down by trapping-detrapping events from the underneath localized states. Furthermore, the energetics of trap states was shown to be affected by surface complexation with electron-donating ligands.⁵⁸⁻⁶⁰ For instance, if the electron density of the ligand is large enough, the electronic levels of the intraband states can be raised into the CB, implying that their trapping action will vanish. The precise shape of the tail states is a delicate issue which is still under discussion.^{19,20,50,61-66} Bisquert and coworkers have found that an exponential density of states below the CB adequately fits several experimental capacitance data.⁶⁷ The proposed DOS shape is:

$$g(E_{Fn}) = \frac{\alpha q N_L}{k_B T} \exp[\alpha(E_{Fn} - E_C)/k_B T] \quad (1)$$

where q is the electronic charge, N_L is the total number of states below the conduction band, k_B is the Boltzmann constant and T is the temperature. E_{Fn} is the Fermi level of the electrons relative to the electrolyte redox potential, and α is an adimensional parameter that, together with the conduction band energy (E_C) describes the DOS distribution. Typical α values lay in the range 0.2-0.5,⁶⁷ although values as small as ~0.05 have also been reported.⁶⁸

Although the effect of trapping states on electron transport in mesoporous nanocrystalline TiO₂ has been extensively investigated,^{3,23,27,36,38,42,69-76} it is still unclear whether these states originate from defects in the bulk and surface regions, from the grain boundaries of the particles, from Coulomb trapping due to interactions of electrons with the cations of the electrolyte, or from a combination of all these factors. Also, TiO₂ nanocrystals

of different shape and size can present different types of defects and of trap states. In contrast to the numerous studies of anatase and rutile low index surfaces,^{77-79,80-82} computational investigations of the structural and electronic properties of TiO₂ nanocrystals (NCs) are still scarce. Density Functional Theory (DFT) was used to study stoichiometric anatase clusters (up to 68 TiO₂ units) with no particular surface orientation,^{83,84} while larger clusters, constituted up to 455 TiO₂ units and with a tetragonal bipyramidal shape, were investigated by Tight-Binding (TB) calculations.⁸⁵ More recently, DFT calculations have been employed to characterize the geometrical and electronic properties of anatase TiO₂ nanoparticles having up to 449 TiO₂ units.⁸⁶ In another DFT study, the electronic structure of pure and Li-doped rutile TiO₂ nanoparticles of up to 61 TiO₂ units, saturated by water molecules was investigated.⁸⁷ The interfaces between two TiO₂ NCs have also been studied, but only via classical molecular dynamics simulations.⁸⁸ The effect of hydrogen bonding on the photoinduced electron transfer and carrier mobility has also been investigated.⁸⁹

In this paper we use quantum mechanical DFT and DFT Tight-Binding (DFTB) calculations to provide an in depth analysis of the nature of trap states in realistic anatase TiO₂ NCs of ca. 3 nm diameter. We consider the effect of the adsorption of donor ligands, specifically H₂O molecules, on the energy and density of trap states of TiO₂ NCs. We further investigate the interaction between two sintered TiO₂ NCs across different interfaces. Our study provides an insight into the nature of trap states in the TiO₂ mesoporous nanocrystalline films employed in DSCs, pointing at the presence of inherent trap states in perfectly stoichiometric and crystalline TiO₂ NCs due to under-coordinated surface Ti(IV) ions at the (100) facets.

2 Computational Details and Calibration

To model realistic TiO₂ NCs containing up to ca. 1500 atoms, we adopt a multi-step computational strategy. We first carry out geometry optimizations by employing self-consistent-charge density-functional tight-binding (SCC-DFTB) methods within the DFTB program.^{90,91} We then perform single point electronic structure calculations on the optimized structures by means of semi-local (i.e. GGA) and non local (i.e. hybrid) DFT within the ADF and PWSCF program packages,⁹²⁻⁹⁴ employing various combinations of basis sets and exchange-correlation functionals, as detailed below. Previous works have shown that DFTB⁹⁵ can predict band structures, geometrical parameters and cohesive energies of anatase polymorphs in good agreement with reference DFT and available experimental data.^{96,97}

For ADF calculations, the local density approximation of Vosko, Wilk, Nusair⁹⁸ (LDA-VWN) augmented with the gradient corrections of Becke⁹⁹ and Perdew¹⁰⁰ (exchange and correlation, respectively, BP86) was employed for most DFT calculations, together with single- ζ (SZ), double- ζ (DZ) and triple- ζ plus polarization functions (TZP) basis sets. Solvent effects have been evaluated through the COSMO solvation model as implemented in the ADF program. A comparison between the GGA-BP86 and the hybrid B3LYP functional was also performed with the ADF program. For PWSCF calculations, we employed the GGA-PBE exchange-correlation functional,¹⁰¹ together with ultrasoft pseudopotentials, as implemented in the Quantum Espresso package.⁹⁴ Plane-wave basis set cutoffs for the smooth part of the

wave functions and the augmented density were 25 and 200 Ry, respectively. A supercell was employed ensuring a minimum separation of 5 Å between periodic images. All the DOS curves have been obtained by a gaussian convolution of width σ , as specified in the various cases (FWHM=2.35 σ).

To check the accuracy of DFTB geometry optimizations, we compared DFT (BP86/DZ) and DFTB optimized structures for a relatively small $(\text{TiO}_2)_{161}\text{-H}_6$ cluster model, see Figure S1, Supporting Information, finding average differences in the Ti-O distances within ~1%. We further checked the quality of DFTB results for the electronic structure of the same $(\text{TiO}_2)_{161}\text{-H}_6$ cluster model, by comparing the DOS obtained by DFTB and BP86/DZ on the DFTB optimized geometry and the DOS obtained by BP86/DZ on the BP86/DZ optimized geometry. The results, Figure S2, Supporting Information, indicate very similar DOS curves for the three methods (the DFTB and BP86/DZ single point energy calculation on the same DFTB geometry give curves that are essentially indistinguishable). We also consider the effect of the basis set dimension and of polarization functions on the unoccupied states of TiO_2 NCs by comparing, for the same $(\text{TiO}_2)_{161}\text{-H}_6$ cluster model at the DFTB-optimized geometry, the DOS obtained by DFTB, PBE/PW, BP86/DZ and BP86/TZP levels of theory. The results, Figure S3, Supporting Information, show very similar DOS curves for the four methods. In particular, the PB86/DZ and BP86/TZP DOS curves are very similar to the PBE/PW DOS curve. What is most relevant to our study, the shape of the DOS tail is essentially the same in the four cases, despite the four methods deliver a different band gap for $(\text{TiO}_2)_{161}\text{-H}_6$ (2.76, 1.64, 1.61 and 1.95 eV for DFTB, BP86/DZ, BP86/TZP and PBE/PW, respectively).

The effect of a polarizable continuum model of solvation on the unoccupied DOS was checked by employing again the $(\text{TiO}_2)_{161}\text{-H}_6$ cluster model at the BP86/DZ level of theory. The results (Figure S4, Supporting Information) show a band gap increase of 0.13 eV and an energy upshift of the HOMO and LUMO (by 0.18 and 0.31 eV, respectively) upon solvation; still, the scaled DOS curves are essentially identical. As an additional check of our approach, we compared the GGA-BP86 and hybrid-B3LYP results for the $(\text{TiO}_2)_{161}\text{-H}_6$ cluster model. Due to the high computational cost of B3LYP calculations, a SZ basis set was used in this case. The resulting DOS curves are shown in Figure S5, Supporting Information. We can see that B3LYP predicts a slightly enhanced DOS in the low energy region. Finally, additional tests show that the agreement between DFTB and PBE/PW results is maintained also for the largest models employed, see Figures S6 and S7, Supporting Information.

Based on the above calibration studies, we have adopted the PBE/PW method to describe the electronic structure of individual NCs, while the less computationally intensive DFTB method has been confidently used to study the electronic structure of water-saturated models and of sintered NCs.

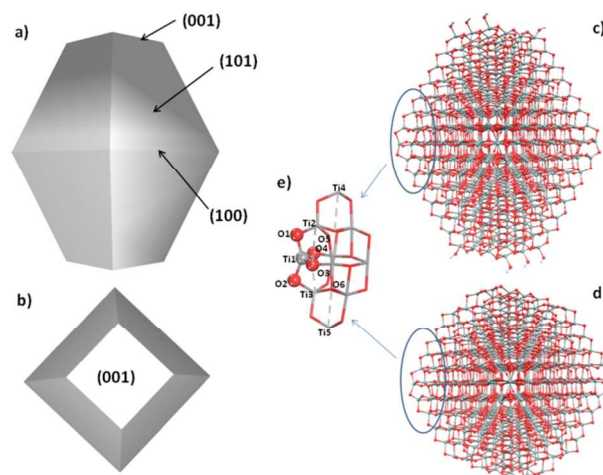
3. Results and discussion

3.1 Structural properties

We generated our starting NC structures by cleaving bulk anatase TiO_2 according the typical bipyramidal Wulff shape. The resulting NCs expose (101) surfaces on the lateral facets, (001)

surfaces on the truncation facets and (100) surfaces at the junction of the two pyramids, see Figure 1. We considered NC models of various sizes, up to 3 nm. After verifying the impossibility to generate perfectly crystalline and stoichiometric, $(\text{TiO}_2)_n$, truncated bipyramidal NCs, we chose to focus on two types of models, obtained by: i) saturating all the under-coordinated dangling oxygen atoms on the (001) surfaces by hydrogen atoms; ii) removing selected atoms from the (101) surfaces to keep the cluster neutral and stoichiometric. In particular, two specific models are discussed in detail in the following: i) a $(\text{TiO}_2)_{411}\text{-H}_{16}$ NC (structure **1** in Figure 1) with perfectly crystalline (101) surfaces and OH-saturated (001) surfaces; ii) a $(\text{TiO}_2)_{367}$ cluster (structure **2** in Figure 1), with some missing atoms ('holes') on the (101) surfaces. The saturation pattern in **1** is justified based on the experimental evidence that anatase surfaces are controlled by acid-base equilibria involving Ti-OH surface hydroxyl groups,¹⁰²⁻¹⁰⁴ while structure **2** is convenient to model the sintering of two NCs and their grain boundaries, since these structure has equally accessible (101) and (001) surfaces. Furthermore, structure **1** is representative of sharp, faceted NCs, while structure **2** is closer to spherical nanoparticles.

Figure 1: a) and b): schematics of the truncated bipyramidal NCs, showing (101), (100) and (001) surfaces from different views. c): optimized geometry of the TiO_2 NC model **1**. d): optimized geometry of the TiO_2 NC model **2**. e): under-coordinated Ti_{4c} at the vertex of the



square basal plane joining two bipyramids together with the neighboring atoms, corresponding to the highlighted region in c) and d). Ti atoms are in grey, O in red and H in white.

The facets of our NC models are characterized by under-coordinated Ti and O atoms with respect to the bulk, where Ti and O atoms have a pseudo-octahedral (Ti_{6c}) and pseudo-trigonal (O_{3c}) coordination, respectively. In particular, for all the considered NC models, five-fold Ti^{4+} (Ti_{5c}) and two-fold coordinated O^{2-} (O_{2c}) sites are present on the (101) and (001) facets, as found on extended surfaces. In addition, four tetracoordinated Ti^{4+} sites (Ti_{4c}), Figure 1, occur on the vertices at the intersection of the four (101) cleavage planes. The under-coordinated Ti_{4c} sites represent an intrinsic characteristic of TiO_2 NCs; e.g., Ti_{4c} sites have been found also in simulated spherical nanoparticles.¹⁰⁵ The presence of under-coordinated Ti_{4c} sites in the TiO_2 mesoporous films and their correlation with trap states for electronic transport has been the subject of various papers by

Teng *et al.*⁷⁴⁻⁷⁶

Upon geometry optimization of **1** and **2**, the largest structural distortions with respect to the bulk crystalline structures occur at the Ti_{4c} under-coordinated sites, which rearrange from the under-coordinated octahedral configuration characteristic of the bulk-truncated structure to a distorted tetragonal configuration. This feature is found in all investigated NC models at all levels of theory employed, thus suggesting that the presence of pseudo-tetrahedral Ti_{4c} sites is a typical feature of these NC structures.

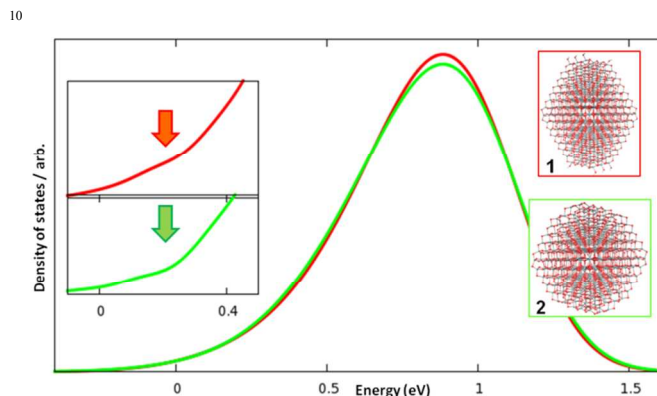


Figure 2. DOS profile (300 lowest unoccupied states) for models **1** (red line) and **2** (green line) calculated at the DFTB optimized geometry with PBE/PW level of theory ($\sigma=0.18$ eV). The two DOS have been aligned at their maximum. The zero of the energy is set at the LUMO of **1**. The inset shows a magnification of the bottom region ($\sigma=0.08$ eV). The arrows in the inset show the region of maximally localized states.

3.2 Electronic structure of individual TiO₂ NCs.

The electronic structure for NCs **1** and **2** computed at the PBE-PW level are compared in terms of DOS in Figure 2, focusing on the manifold of unoccupied states.

Similar band gaps of 1.68 (2.71) and 1.79 (2.83) eV were computed for **1** and **2** by PBE-PW (DFTB), respectively. The PBE-PW calculated band gaps are considerably underestimated compared to the 3.2 eV experimental band gap of anatase. This discrepancy could be reduced by the use of computationally convenient DFT+U methods,^{81,106} that however are strongly dependent from the choice of the U value, or by employing hybrid functional with a variable fraction of Hartree-Fock exchange,¹⁰⁷⁻¹⁰⁹ which are however too computationally expensive to be used here. Since the focus of the present work is mainly on comparing the density of unoccupied states of different NC models, we expect the present level of theory to be sufficiently accurate for comparative purposes. The slightly smaller, 0.11 eV (0.12 eV), band gap of **1** compared to **2** is due to an energy up-shift of the valence band (VB) maximum, which is mainly caused by the electron-donor properties of the OH⁻ groups. In the following we focus on NC **1**, resorting again to **2** for the discussion of the effect of sintering.

To compare the calculated DOS for **1** with available experimental capacitance measurements on dye-sensitized TiO₂, we fitted our data to equation 1 in its logarithmic form. As shown in Figure 3, very good linear fits ($R^2=0.99$) were obtained in an energy range ca. 0.1-0.6 eV above the LUMO. Below 0.1 eV, a few localized states are found, while above this energy range the DOS of our models changes its shape and slope due to the finite

system's dimension. Also notice that although a Gaussian broadening has been used to calculate the DOS, this should not directly influence the fit, which does not include the tail below the LUMO originated by the broadening. The resulting α and E_c values (cf. eq. 1) for NC **1** are 0.13 and 0.35 eV (at T=300 K). Although this value of α is on the lower edge of measured data, the result is remarkable, considering the relative simplicity of our model.

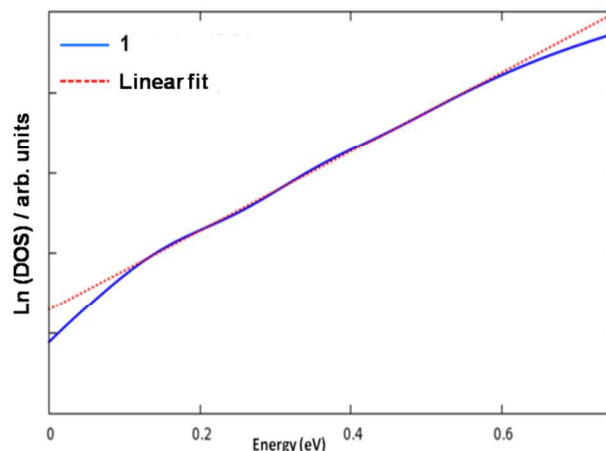


Figure 3. Linear fit ($a=\alpha$, $b=-E_c$) of log data obtained from the DOS of NC **1** calculated at the PBE/PW level of theory ($\sigma=0.08$ eV). The zero of the energy is set at the LUMO.

The unoccupied states of lowest energy for NC **1**, of titanium t_{2g} character, are localized within the central part of the NC, mainly at the intersection of the (100) and (101) surfaces, see left panel of Figure 4. We note that a different LUMO was found in Reference 86 for sharp- and flat-shaped NCs, using TiO₂ NC models with a different saturation scheme of dangling Ti and O atoms. At higher energy, the unoccupied states are progressively more delocalized, with the lowest energy state completely delocalized over the NC structure (right panel of Figure 4) being found ca. 0.3-0.4 eV above the LUMO, in agreement with both electrochemical and spectro-electrochemical results,^{23-25,35} and with the data fit analysis presented above.

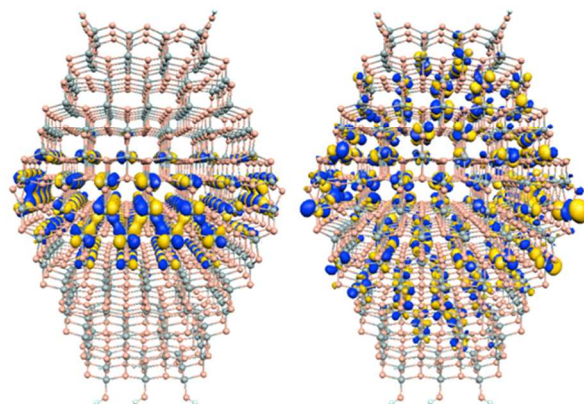


Figure 4. Representative unoccupied states characterizing the LUMO (left) and the higher energy CB states, at ca. 0.3-0.4 eV above the LUMO (right).

To check the sensitivity of the low-energy states at the bottom of the DOS to external ligands, we optimized the geometry of

model **1** after adding 154 surface-adsorbed H₂O molecules. We found that the surface saturation in **1/H₂O** gives rise to an energy up-shift of both the VB and CB edge of ca. 0.5 eV at the DFTB level, see Figure S8, Supporting Information. Such shift is perfectly coherent with the decrease of the work function experimentally observed upon hydration of TiO₂ surfaces,¹¹⁰ and was also found for rutile nanoparticles in Ref.⁸⁷. Surface-adsorbed H₂O molecules raise the energy and reduce the number of localized states at the bottom of the unoccupied DOS, Figure 5. In fact, the DOS curve for **1/H₂O** is not simply shifted to higher energy compared to that calculated for **1**, but has an evidently different curvature. We also note that some localized trap states are still found in **1/H₂O**, since the Ti_{4c} sites on the (100) surfaces are not entirely saturated by water molecules and maintain a weak 5-fold coordination, with average computed Ti-OH₂ distances of 2.90 Å.

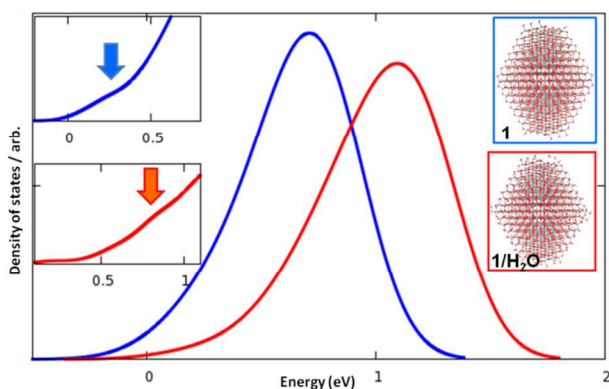


Figure 5. DOS profile (300 lowest unoccupied states) for models **1** (blue line) and **1/H₂O** (red line) calculated at the DFTB level of theory ($\sigma=0.18$ eV). The zero of the energy is set at the LUMO of **1**. The inset shows a magnification of the bottom region ($\sigma=0.08$ eV). The arrows in the inset show the region of maximally localized states.

To provide a quantitative picture of the unoccupied state energy localization within the considered TiO₂ NCs, we report in Figure 6 a contour plot of the space/energy diagram for system **1**. This diagram is obtained by scanning the NC along the main longitudinal axis and summing up the contributions of each atom to a given unoccupied state as a function of the energy state. In line with the qualitative analysis presented above, this diagram shows a substantial contribution to the low-energy portion of the DOS from states which are mainly localized on the central NC part. By increasing the energy, the states become progressively more delocalized over the entire NC structure, with the top/bottom (001) facets maximally contributing to the high energy portion of the DOS. Similar plots are obtained for NC **2**, see Figure S9, Supporting Information. The results can be visualized in the pictorial representation of the space/energy distribution in NC **1** shown on the right of Figure 6. The localized surface states constituting the bottom of the DOS for the observed TiO₂ NC clearly constitute trapping sites for electron transport, and may further represent recombination sites between injected electrons and oxidized species in the electrolyte.

3.3 Sintered Nanocrystals

To investigate whether the boundaries between sintered NCs can introduce electronic trap states at the bottom of the unoccupied states manifold, we constructed models of sintered NCs by attaching two TiO₂ NCs at their available surfaces. The optimized structures of two NCs of type **2** with 101/101, 101/001, 001/001 and 100/001 interfaces are shown in Figure 7. The same picture holds for NCs of type **1**, for which we modeled only the 101/101 interface only, see Figure S10, Supporting Information. We found that sintering of two NCs at their 101/101 surfaces is the most effective, leading to a DFTB-calculated stabilization energy of 28.6 eV relative to two non-interacting NCs. This value reduces to 9.1, 7.1 and 6.6 eV for 101/001, 001/001 and 100/001 interfaces, respectively.

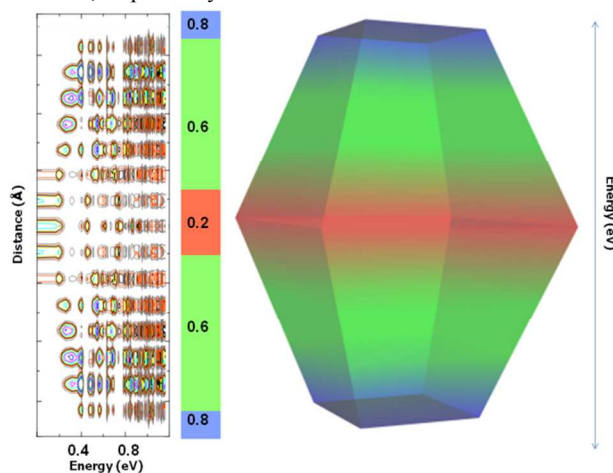


Figure 6. Contour plot of the space/energy (eV) diagram for the DOS of unoccupied states of NC **1**, scanned along the length of the NC. Three DOS areas are identified, corresponding to the central, intermediate and top/bottom NC regions. The right panel shows a pictorial representation of such space/energy diagram, with colors shifting from red to green to blue indicating localization in the related colored region of states of increasing energy.

The larger stabilization energy found for the 101/101 interface is due to the larger accessible surface available and to the almost optimal structural matching that is observed at the interface between the two interacting NCs, see Figure 7. When normalizing the calculated interaction energies by the interface area, we find values of 0.14, 0.05, 0.08 and 0.09 eV/Å for 101/101, 101/001, 001/001 and 001/001 interactions, respectively, indicating that the 101/101 interaction is the most favorable one irrespective of the available surface area. The strength of the interaction is due to the number of Ti-O bonds that are formed upon sintering, within the limits imposed by the morphology of the NCs. We also note that the formation of Ti-O bonds between two NCs causes the saturation of only few under-coordinated Ti sites, so that the effect of sintering on the distribution of the surface trap states of individual NCs is expected to be quite limited.

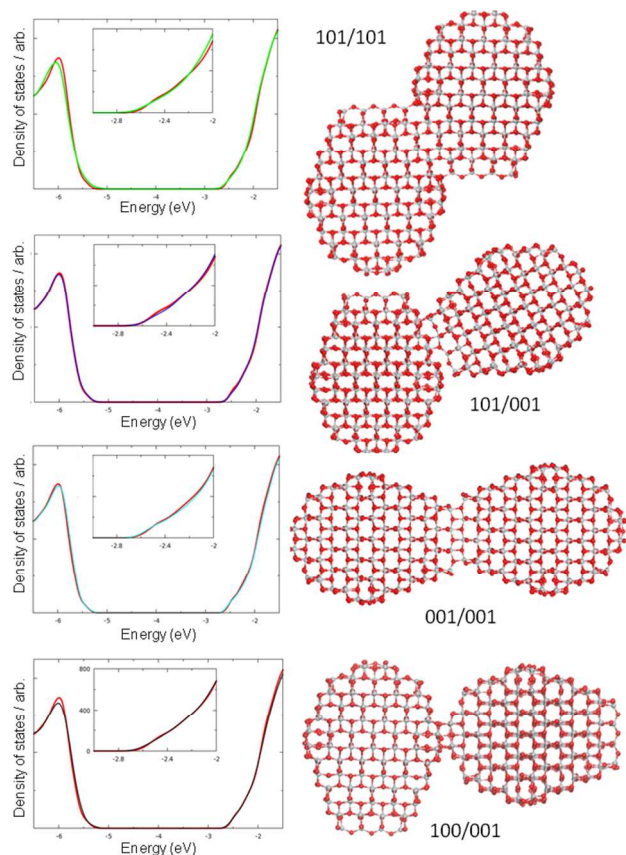


Figure 7. Optimized geometries for two interacting NCs (model 2) with the 101/101, 101/001, 001/001 and 100/001 interfaces, along with the corresponding DOS (curves of different colors) compared to that of the isolated model 2 (red curves) calculated at the DFTB level of theory ($\sigma=0.18$ eV).

The computed DOS for the sintered configurations confirms that the shape of the DOS tail is not largely affected by the NCs boundaries, while subtle differences in the distribution of the trap states are found for those configurations where some under-coordinated Ti sites are saturated, such as the 101/101 and 100/001 models in Figure 7. These results indicate that, upon full relaxation, the structure of two interacting NCs tends to become similar to a bulk like structure. Obviously, this might not always be the case under the high temperature/short time conditions used experimentally for NC film sintering (500 C for 1/2 hour), also considering that at that temperature the ligands surrounding the NCs are destroyed, thus adding an additional level of disorder to the NCs interactions.

4 Conclusions

We have used quantum mechanical calculations based on DFT and DFTB methods to investigate the nature of electronic trap states in realistic models of sintered and individual anatase TiO₂ NCs of ca. 3 nm diameter. We found the unoccupied states of lowest energy, of titanium t_{2g} character, to be specifically localized within the central part of the investigated NCs. These states originate from under-coordinated 4-fold coordinated surface Ti atoms mainly lying at the (100) edges found at the intersections between (101) surfaces. At higher energy, the

unoccupied states get progressively more delocalized, with the lowest energy state completely delocalized over the NC structure signaling the system's conduction band (CB). The localized states give rise to an exponential DOS tail which is found 0.3-0.4 eV below the fully delocalized CB states, in excellent agreement with both electrochemical, spectro-electrochemical and capacitance data.

The effect of the adsorption of donor ligands (specifically H₂O molecules) on the energy and density of traps states of TiO₂ NCs was also considered. We found that surface saturation substantially alters the NC electronic structure, with a computed energy up-shift of both the VB and CB edge of ca. 0.5 eV, in agreement with the decrease of the work function experimentally observed upon hydration of TiO₂ surfaces. The adsorbed water molecules reduces also the number of localized states at the bottom of the manifold of unoccupied states, thus modifying the DOS shape.

Finally, the interaction between two sintered TiO₂ NCs was investigated by considering attachment at all the possible surface combinations. Interestingly, no major effects on the joint DOS of two interacting NCs was found compared to that of the individual, constituent NCs. Although our calculations did not consider the role of defects, e.g. oxygen vacancies, and for sintered NCs did not include the disorder which is expected to characterize the TiO₂ film formation under typical DSSCs fabrication conditions, our results clearly point at the presence of inherent trap states even in perfectly stoichiometric and crystalline TiO₂ NCs due to the unavoidable presence of 4-fold coordinated surface Ti(IV) ions. Our results constitute the basis for building specifically tailored TiO₂ nanostructures which may lead to enhanced DSCs efficiency, by virtue of enhanced transport properties, and provide insight into the effect of surface-passivating layers in reducing recombination reactions in DSCs.

Acknowledgment: The authors thank FP7-NMP-2009 Project 246124 "SANS" for financial support. A.S. thanks the support of DoE-BES, Chemical Sciences, Geosciences and Biosciences Division, Contract No. DE-FG02-12ER16286. The authors thank Dr. Rinaldo Psaro for useful discussions.

Notes and references

^a Computational Laboratory of Hybrid/Organic Photovoltaics (CLHYO), Istituto CNR di Scienze e Tecnologie Molecolari, via Elce di Sotto 8, I-06123 Perugia, Italy. Fax: +39 075 5855606; Tel: +39 075 5855523; E-mail: filippo@thch.unipg.it

^b Dipartimento di Chimica, Università degli Studi di Perugia, via Elce di Sotto 8, I-06123 Perugia, Italy. Fax: +39 075 5855606; Tel: +39 075 5855517; E-mail: nunzi@thch.unipg.it

^c Dipartimento di Farmacia, Università G. D'Annunzio, via dei Vestini 31, 66100 Chieti, Italy.

^d Department of Chemistry, Princeton University, Princeton, NJ-08544, USA.

^e Laboratory of Photonics and Interfaces, Institute of Chemical Sciences and Engineering, Faculty of Basic Science, Ecole Polytechnique Fédérale de Lausanne, CH-1015 Lausanne, Switzerland.

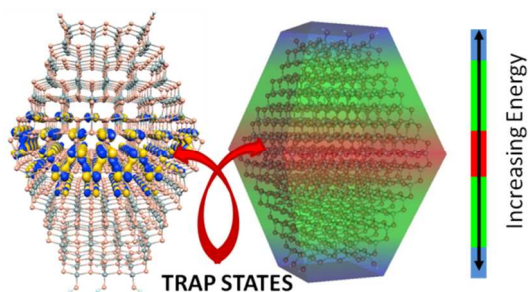
† Electronic Supplementary Information (ESI) available: optimized structures and DOS curves. See DOI: 10.1039/b000000x/

1 B. O'regan and M. Grätzel, *Nature*, 1991, **353**, 737-740.

- 2 J.M. Rehm, G.L. Mclendon, Y. Nagasawa, K. Yoshihara, J. Moser and M. Gratzel, *J. Phys. Chem. B*, 1996, **100**, 9577-9578.
- 3 A. Hagfeldt and M. Grätzel, *Chem. Rev.*, 1995, **95**, 49-68.
- 4 M. Graetzel, *Nature*, 2001, **414**, 338-344.
- 5 5 A. Hagfeldt, G. Boschloo, L. Sun, L. Kloo and H. Pettersson, *Chem. rev.*, 2010, **110**, 6595-6663.
- 6 A. Yella, H.-W. Lee, H.N. Tsao, C. Yi, A.K. Chandiran, M.K. Nazeeruddin, E.W.-G. Diao, C.-Y. Yeh, S.M. Zakeeruddin and M. Grätzel, *Science*, 2011, **334**, 629-634.
- 10 7 G. Schlichthörl, N.G. Park and A.J. Frank, *J. Phys. Chem. B*, 1999, **103**, 782-791.
- 8 J. Van De Lagemaat, N.G. Park and A.J. Frank, *J. Phys. Chem. B*, 2000, **104**, 2044-2052.
- 9 F. Cao, G. Oskam, G.J. Meyer and P.C. Searson, *J. Phys. Chem. B*, 1996, **100**, 17021-17027.
- 15 10 L. Dloczik, O. Ieperuma, I. Lauer mann, L.M. Peter, E.A. Ponomarev, G. Redmond, N.J. Shaw and I. Uhlen dorf, *J. Phys. Chem. B*, 1997, **101**, 10281-10289.
- 11 P.E. De Jongh and D. Vanmaekelbergh, *J. Phys. Chem. B*, 1997, **101**, 2716-2722.
- 20 12 J. Bisquert, G. Garcia-Belmonte and F. Fabregat-Santiago, *J. Solid State Electrochem.*, 1999, **3**, 337-347.
- 13 J. Bisquert, *J. Phys. Chem. B*, 2002, **106**, 325-333.
- 14 A. Solbrand, H. Lindstrom, H. Rensmo, A. Hagfeldt, S.E. Lindquist and S. Sodergren, *J. Phys. Chem. B*, 1997, **101**, 2514-2518.
- 25 15 B. O'regan, J. Moser, M. Anderson and M. Grätzel, *J. Phys. Chem.*, 1990, **94**, 8720-8726.
- 16 S. Sodergren, A. Hagfeldt, J. Olsson and S.E. Lindquist, *J. Phys. Chem.*, 1994, **98**, 5552-5556.
- 30 17 J. Bisquert, *J. Phys. Chem. B*, 2004, **108**, 2323-2332.
- 18 N. Kopidakis, E.A. Schiff, N.G. Park, J. Van De Lagemaat and A.J. Frank, *J. Phys. Chem. B*, 2000, **104**, 3930-3936.
- 19 F. Fabregat-Santiago, I. Mora-Sero, G. Garcia-Belmonte and J. Bisquert, *J. Phys. Chem. B*, 2003, **107**, 758-768.
- 35 20 J. Bisquert, F. Fabregat-Santiago, I. Mora-Sero, G. Garcia-Belmonte, E.M. Barea and E. Palomares, *Inorg. Chim. Acta*, 2008, **361**, 684-698.
- 21 J.M. Montero and J. Bisquert, *Solid State Electron.*, 2011, **55**, 1-4.
- 40 22 J. Bisquert, F. Fabregat-Santiago, I. Mora-Sero, G. Garcia-Belmonte and S. Gimenez, *J. Phys. Chem. C*, 2009, **113**, 17278-17290.
- 23 J. Bisquert, A. Zaban and P. Salvador, *J. Phys. Chem. B*, 2002, **106**, 8774-8782.
- 24 J. Bisquert and V.S. Vikhrenko, *J. Phys. Chem. B*, 2004, **108**, 2313-2322.
- 45 25 A. Zaban, M. Greenshtein and J. Bisquert, *Chem. Phys. Chem.*, 2003, **4**, 859-864.
- 26 M. Bailes, P.J. Cameron, K. Lobato and L.M. Peter, *J. Phys. Chem. B*, 2005, **109**, 15429-15435.
- 50 27 S. Ardo and G.J. Meyer, *Chem. Soc. Rev.*, 2009, **38**, 115-164.
- 28 A. Hagfeldt and L. Peter *Dye-sensitized Solar Cells* EPFL Press: Lausanne, 2010.
- 29 J.E. Moser *Dye-sensitized Solar Cells* EPFL Press: Lausanne, 2010.
- 55 30 T.L. Thompson and J.T. Yates, *Chem. Rev.*, 2006, **106**, 4428-4453.
- 31 R.F. Howe and M. Grätzel, *J. Phys. Chem.*, 1985, **89**, 4495-4499.
- 32 R.F. Howe and M. Grätzel, *J. Phys. Chem.*, 1987, **91**, 3906-3909.
- 60 33 M. Graetzel and R.F. Howe, *J. Phys. Chem.*, 1990, **94**, 2566-2572.
- 34 W. Siripala and M. Tomkiewicz, *J. Electrochem. Soc.*, 1982, **129**, 1240-1245.
- 65 35 J. Bisquert, A. Zaban, M. Greenshtein and I. Mora-Serò, *J. Am. Chem. Soc.*, 2004, **126**, 13550-13559.
- 36 K. Westermark, A. Henningsson, H. Rensmo, S. Sodergren, H. Siegbahn and A. Hagfeldt, *Chem. Phys.*, 2002, **285**, 157-165.
- 37 D. Fitzmaurice, *Sol. Energy Mater. Sol. Cells*, 1994, **32**, 289-305.
- 70 38 G. Rothenberger, D. Fitzmaurice and M. Grätzel, *J. Phys. Chem.*, 1992, **96**, 5983-5986.
- 39 L. Kavan, K. Kratochvilová and M. Grätzel, *J. Electroanal. Chem.*, 1995, **394**, 93-102.
- 75 40 G. Boschloo and D. Fitzmaurice, *J. Phys. Chem. B*, 1999, **103**, 2228-2231.
- 41 H. Wang, J. He, G. Boschloo, H. Lindstrom, A. Hagfeldt and S.-E. Lindquist, *J. Phys. Chem. B*, 2001, **105**, 2529-2533.
- 42 N. Kopidakis, N.R. Neale, K. Zhu, J. Van De Lagemaat and A.J. Frank, *Appl. Phys. Lett.*, 2005, **87**, 202106-202108.
- 43 T. Berger, M. Sterrer, O. Diwald, E. Knözinger, D. Panayotov, T.L. Thompson and J.T. Yates, *J. Phys. Chem. B*, 2005, **109**, 6061-6068.
- 44 T. Berger, T. Lana-Villarreal, D. Monllor-Satoca and R. Gómez, *Electrochem. Commun.*, 2006, **8**, 1713-1718.
- 85 45 L. De La Garza, Z.V. Saponjic, N.M. Dimitrijevic, M.C. Thurnauer and T. Rajh, *J. Phys. Chem.*, 2005, **110**, 680-686.
- 46 A. Usami and H. Ozaki, *J. Phys. Chem. B*, 2001, **105**, 4577-4583.
- 47 J. Bisquert, D. Cahen, G. Hodes, S. Ruhle and A. Zaban, *J. Phys. Chem. B*, 2004, **108**, 8106-8118.
- 90 48 L.M. Peter, N.W. Duffy, R.L. Wang and K.G.U. Wijayantha, *J. Electroanal. Chem.*, 2002, **524**, 127-136.
- 49 V.G. Kytin, J.P. Gonzalez-Vazquez, J.A. Anta and J. Bisquert, *IEEE J. Sel. Top. Quantum Electron.*, 2010, **16**, 1581-1586.
- 95 50 J.R. Durrant, *J. Photochem. Photobiol. A: Chem.*, 2002, **148**, 5-10.
- 51 P.E. De Jongh and D. Vanmaekelbergh, *Phys. Rev. Lett.*, 1996, **77**, 3427-3430.
- 52 J.R. Durrant, S.A. Haque and E. Palomares, *Coord. Chem. Rev.*, 2004, **248**, 1247-1257.
- 53 J. Nelson, S.A. Haque, D.R. Klug and J.R. Durrant, *Phys. Rev. B*, 2001, **63**, 205321.
- 54 J. Nelson, *Phys. Rev. B*, 1999, **59**, 15374.
- 55 J. Nelson and R.E. Chandler, *Coord. Chem. Rev.*, 2004, **248**, 1181-1194.
- 105 56 J. Bisquert, *Phys. Chem. Chem. Phys.*, 2008, **10**, 3175-3194.
- 57 J. Bisquert, *J. Electroanal. Chem.*, 2010, **646**, 43-51.
- 58 J. Moser, S. Punehihewa, P.P. Infelta and M. Grätzel, *Langmuir*, 1991, **7**, 3012-3018.
- 110 59 G. Redmond, D. Fitzmaurice and M. Grätzel, *J. Phys. Chem.*, 1993, **97**, 6951-6954.

- 60 N.M. Dimitrijevic, Z.V. Saponjic, D.M. Bartels, M.C. Thurnauer, D.M. Tiede and T. Rajh, *J. Phys. Chem. B*, 2003, **107**, 7368-7375.
- 61 I. Abayev, A. Zaban, V.G. Kytin, A.A. Danilin, G. Garcia-Belmonte and J. Bisquert, *J. Solid State Electr.*, 2007, **11**, 647-653.
- 62 A.J. Morris and G.J. Meyer, *J. Phys. Chem. B*, 2008, **112**, 18224-18231.
- 63 J. Van De Lagemaat, N. Kopidakis, N.R. Neale and A.J. Frank, *Phys. Rev. B*, 2005, **71**, 035304.
- 64 S.A. Haque, E. Palomares, B.M. Cho, A.N.M. Green, N. Hirata, D.R. Klug and J.R. Durrant, *J. Am. Chem. Soc.*, 2005, **127**, 3456-3462.
- 65 Y. Tachibana, I.V. Rubtsov, I. Montanari, K. Yoshihara, D.R. Klug and J.R. Durrant, *J. Photochem. Photobiol. A: Chem.*, 2001, **142**, 215-220.
- 66 V.G. Kytin, J. Bisquert, I. Abayev and A. Zaban, *Phys. Rev. B*, 2004, **70**, 193304.
- 67 F. Fabregat-Santiago, G. Garcia-Belmonte, I. Mora-Sero and J. Bisquert, *Phys. Chem. Chem. Phys.*, **13**, 9083-9118.
- 68 J.R. Jennings, A. Ghicov, L.M. Peter, P. Schmuki and A.B. Walker, *J. Am. Chem. Soc.*, 2008, **130**, 13364-13372.
- 69 A. Kay, R. Humphry-Baker and M. Graetzel, *J. Phys. Chem.*, 1994, **98**, 952-959.
- 70 B.A. Gregg, S.G. Chen and S. Ferrere, *J. Phys. Chem. B*, 2003, **107**, 3019-3029.
- 71 G. Boschloo and A. Hagfeldt, *Chem. Phys. Lett.*, 2003, **370**, 381-386.
- 72 A.C. Fisher, L.M. Peter, E.A. Ponomarev, A.B. Walker and K.G.U. Wijayantha, *J. Phys. Chem. B*, 2000, **104**, 949-958.
- 73 D.S. Zhang, J.A. Downing, F.J. Knorr and J.L. Mchale, *J. Phys. Chem. B*, 2006, **110**, 21890-21898.
- 74 P.-T. Hsiao and H. Teng, *J. Am. Ceram. Soc.*, 2009, **92**, 888-893.
- 75 P.-T. Hsiao, Y.-L. Tung and H. Teng, *J. Phys. Chem. C*, 2011, **114**, 6762-6769.
- 76 Y.-J. Liou, P.-T. Hsiao, L.-C. Chen, Y.-Y. Chu and H. Teng, *J. Phys. Chem. C*, 2012, **115**, 25580-25589.
- 77 U. Diebold, *Surf. Sci. Rep.*, 2003, **48**, 53-229.
- 78 A. Vittadini, A. Selloni, F.P. Rotzinger and M. Gratzel, *Phys. Rev. Lett.*, 1998, **81**, 2954.
- 79 U. Diebold, N. Ruzicky, G.S. Herman and A. Selloni, *Catal. Today*, 2003, **85**, 93-100.
- 80 E. Finazzi, C. Di Valentin and G. Pacchioni, *J. Phys. Chem. C*, 2009, **113**, 3382-3385.
- 81 E. Finazzi, C. Di Valentin, G. Pacchioni and A. Selloni, *J. Chem. Phys.*, 2008, **129**, 154113.
- 82 P. Krüger, S. Bourgeois, B. Domenichini, H. Magnan, D. Chandris, P. Le Fèvre, A.M. Flank, J. Jupille, L. Floreano, A. Cossaro, A. Verdini and A. Morgante, *Phys. Rev. Lett.*, 2008, **100**, 055501.
- 83 M.J. Lundqvist, M. Nilsing, P. Persson and S. Lunell, *Int. J. Quantum Chem.*, 2006, **106**, 3214-3234.
- 84 A. Iacomino, G. Cantele, D. Ninno, I. Marri and S. Ossicini, *Phys. Rev. B*, 2008, **78**, 075405.
- 85 A.S. Barnard, S. Erdin, Y. Lin, P. Zapol and J.W. Halley, *Phys. Rev. B*, 2006, **73**, 205405.
- 86 Y.-F. Li and Z.-P. Liu, *J. Am. Chem. Soc.*, 2011, **133**, 15743-15752.
- 87 J. Zhang, T.F. Hughes, M. Steigerwald, L. Brus and R.A. Friesner, *J. Am. Chem. Soc.*, 2012, **134**, 12028-12042.
- 88 a) V.N. Koparde and P.T. Cummings, *ACS Nano*, 2008, **2**, 1620-1624; b) M. Alimohammadi and K.A. Fichtthorn, *Nano Lett.*, 2009, **9**, 4198-4203.
- 89 a) G.-J. Zhao, K.-L. Kan *Acc. Chem. Res.*, 2012, **45**, 404-413; b) G.-J. Zhao, J.-Y. Liu, L.-C. Zhou, K.-L. Kan *J. Phys. Chem. B*, 2007, **111**, 8940-8945.
- 90 M. Elstner, D. Porezag, G. Jungnickel, J. Elsner, M. Haugk, T. Frauenheim, S. Suhai and G. Seifert, *Phys. Rev. B*, 1998, **58**, 7260-7268.
- 91 B. Aradi, B. Hourahine and T. Frauenheim, *J. Phys. Chem. A*, 2007, **111**, 5678-5684.
- 92 E.J. Baerends, D.E. Ellis and P. Rosa, *Chem. Phys.*, 1973, **2**, 41.
- 93 C.F. Guerra, J.G. Snijders, G. Te Velde and E.J. Baerends, *Theor. Chem. Acc.*, 1998, **99**, 391-403.
- 94 P. Giannozzi; <http://www.quantum-espresso.org>; et al.
- 95 G. Seifert, *J. Phys. Chem. A*, 2007, **111**, 5609.
- 96 G. Dolgonos, B. Aradi, N.H. Moreira and T. Frauenheim, *J. Chem. Theory Comput.*, 2010, **6**, 266-278.
- 97 H. Fox, K.E. Newman, W.F. Schneider and S.A. Corcelli, *J. Chem. Theory Comput.*, **6**, 499-507.
- 98 S.H. Vosko, L. Wilk and M. Nusair, 1980, **58**, 1200.
- 99 A.D. Becke, *Phys. Rev.*, 1988, **A38**, 2398.
- 100 J.P. Perdew, *Phys. Rev.*, 1986, **B33**, 8822.
- 101 J.P. Perdew, K. Burke and M. Ernzerhof, *Phys. Rev. Lett.*, 1996, **77**, 3865-3868.
- 102 Y. Nakaoka and Y. Nosaka, *J. Photochem. Photobiol. A-Chem.*, 1997, **110**, 299-305.
- 103 S.H. Szczepankiewicz, J.A. Moss and M.R. Hoffmann, *J. Phys. Chem. B*, 2002, **106**, 7654-7658.
- 104 Z.V. Saponjic, N.M. Dimitrijevic, D.M. Tiede, A.J. Goshe, X. Zuo, L.X. Chen, A.S. Barnard, P. Zapol, L. Curtiss and T. Rajh, *Adv. Mater.*, 2005, **17**, 965-971.
- 105 P.K. Naicker, P.T. Cummings, H. Zhang and J.F. Banfield, *J. Phys. Chem. B*, 2005, **109**, 15243-15249.
- 106 Z. Hu and H. Metiu, *J. Phys. Chem. C*, 2011, **115**, 5841-5845.
- 107 F. De Angelis, S. Fantacci, A. Selloni, M.K. Nazeeruddin and M. Grätzel, *J. Phys. Chem. C*, 2010, **114**, 6054-6061.
- 108 C. Di Valentin, G. Pacchioni and A. Selloni, *Phys. Rev. Lett.*, 2006, **97**.
- 109 N.M. Harrison, X.G. Wang, J. Muscat and M. Scheffler, 1999, **114**, 305.
- 110 Y.B. He, A. Tilocca, O. Dulub, A. Selloni and U. Diebold, *Nat. Mater.*, 2009, **8**, 585-589.

TOC Graphics:



TOC text:

Quantum mechanical investigations on realistic anatase TiO₂ nanocrystals reveal the presence of inherent trap states localized on the (100) facets.

Broader Context:

Dye-sensitized solar cells (DSCs) are based on a mesoporous semiconductor oxide composed by a network of sintered nanoparticles, sensitized by a dye and interpenetrated by a redox shuttle. Electron transport in the mesoporous film is usually orders of magnitude slower than in the corresponding single crystals, suggesting a high concentration of traps. Since electron transport competes in with recombination, understanding the nature of the transport-limiting traps could further advance the DSCs technology.

We report a quantum mechanical investigation of the nature of trap states in realistic anatase TiO₂ nanocrystals of ca. 3 nm diameter, exploring the effect of surface saturation and of nanoparticle sintering. Our results point at the presence of inherent trap states in perfectly stoichiometric and crystalline TiO₂ nanocrystals, due to under-coordinated surface Ti(IV) ions at the (100) facets. These trap states are largely removed by surface saturation, while the effect of sintering between two nanocrystals is found to introduce minor modifications in the electronic structure compared to that of individual nanocrystals.

Our results constitute the basis for building specifically tailored TiO₂ nanostructures which may lead to enhanced DSCs efficiency, and provide insight into the effect of surface-passivating layers in reducing recombination reactions in DSCs.

30